

Here, $453M(C)$ is a mobility, w is the so-called gradient energy coefficient, and the gradients are taken with respect to arc length. The first term on the right-hand side describes the chemical effect leading to phase separation within the spinodal; the second term describes the effect that damps short-wavelength fluctuations. The mobility is proportional to the surface diffusivity D_s and is given by $M(C) = (D_s/k_B T)c(1-c)$. The mobility is peaked for $c = 0.5$, and is zero for $c = 0$ and $c = 1$ (atoms do not diffuse in pure phases because there are no vacancies in our model). The normal velocity is given by $v_n(C) = V(C)[1 - (\gamma\Omega/k_B T)\kappa]$, where γ is the surface free energy and $V(C)$ is called the interface response function, equal to the velocity of a flat surface covered with a concentration C of gold. We find in both simulation and experiment that the interface response is fitted well by the functional form $V(C) = V_0(\phi)\exp(-C/C^*)$, where ϕ is the overpotential and C^* is a constant. Experimentally, the gold accumulation can be inferred by integrating the dissolution current versus time at fixed overpotential; it is necessary to use an overpotential that is low enough to ensure that the surface remains planar (that is, porosity does not form) and also to catch the short initial transient rise in current as silver atoms are pulled from the first few monolayers. This particular form for the interface response function is quite curious. Naively, one might expect that the local interface velocity would be proportional to the local concentration of silver exposed to the electrolyte, that is, $V(C) \propto (1-c)$. However, the decaying exponential form suggests that there is an evolving distribution of holes opening and closing within the interfacial region, controlling the accumulation rate.

Physically, the mass conservation condition (equation (1)) is the statement that the total number $Cb\Delta s$ of gold atoms in a length Δs of interface with lateral width b can change as a result of three distinct effects that correspond to the three terms on the right-hand-side of equation (1): the accumulation of gold atoms into the interfacial layer from the solid being dissolved; the local stretching of the interface ($\partial\Delta s/\partial t = v_n\kappa\Delta s$), which can either increase or decrease C depending on whether the solid is concave ($\kappa > 0$) or convex ($\kappa < 0$); and the motion of atoms along the interface driven by the surface diffusion flux J_s .

Received 14 November 2000; accepted 10 January 2001.

- Pickering, H. W. Characteristic features of alloy polarization curves. *Corros. Sci.* **23**, 1107–1120 (1983).
- Forty, A. J. Corrosion micromorphology of noble metal alloys and depletion gilding. *Nature* **282**, 597–598 (1979).
- Masing, G. Zur Theorie der Resistenzgrenzen in Mischkristallen. *Z. Anorg. Allg. Chem.* **118**, 293–308 (1921).
- Lechtman, H. Pre-Columbian surface metallurgy. *Sci. Am.* **250**, 56–63 (1984).
- Williams, D. E., Newman, R. C., Song, Q. & Kelly, R. G. Passivity breakdown and pitting corrosion of binary alloys. *Nature* **350**, 216–219 (1991).
- Newman, R. C. & Sieradzki, K. Metallic Corrosion. *Science* **263**, 1708–1709 (1994).
- Li, R. & Sieradzki, K. Ductile-brittle transition in random porous Au. *Phys. Rev. Lett.* **68**, 1168–1171 (1992).
- Corcoran, S. in *Critical Factors in Localized Corrosion III* (eds Kelly, R. G., Frankel, G. S., Natishan, P. M. & Newman, R. C.) 500–507 (Electrochemical Society, Pennington, New Jersey, 2000).
- Pickering, H. W. & Wagner, C. Electrolytic dissolution of binary alloys containing a noble metal. *J. Electrochem. Soc.* **114**, 698–706 (1967).
- Sieradzki, K., Corderman, R. R., Shukla, K. & Newman, R. C. Computer simulations of corrosion: selective dissolution of binary alloys. *Phil. Mag. A* **59**, 713–746 (1989).
- Sieradzki, K. Curvature effects in alloy dissolution. *J. Electrochem. Soc.* **140**, 2868–2872 (1993).
- Wagner, C. Contribution to the theory of electropolishing. *J. Electrochem. Soc.* **101**, 225–228 (1953).
- Erlebacher, J. in *Dynamics of Crystal Surfaces and Interfaces* (eds Duxbury, P. & Pence, T.) 24–28 (Plenum, New York, 1997).
- Wagner, K., Brankovic, S. R., Dmitrov, N. & Sieradzki, K. Dealloying below the critical potential. *J. Electrochem. Soc.* **144**, 3545–3555 (1997).
- Cahn, J. W. & Hilliard, J. E. Free energy of a nonuniform system. I. Interfacial free energy. *J. Chem. Phys.* **28**, 258–267 (1958).
- Cahn, J. W. & Hilliard, J. E. Free energy of a nonuniform system. III. Nucleation in a two-component incompressible fluid. *J. Chem. Phys.* **31**, 688–699 (1958).
- Hilliard, J. E. in *Solidification* 497–560 (American Society for Metals, Metals Park, Ohio, 1971).
- Ben-Jacob, E., Goldenfeld, N., Langer, J. S. & Schon, G. Dynamics of interfacial pattern formation. *Phys. Rev. Lett.* **51**, 1930–1932 (1983).
- Mullins, W. W. Theory of thermal grooving. *J. Appl. Phys.* **28**, 333–339 (1957).
- Kessler, D. A., Koplik, J. & Levine, H. Geometrical models of interface evolution. II. Numerical simulation. *Phys. Rev. A* **30**, 3161–3174 (1984).
- Hou, T. Y., Lowengrub, J. S. & Shelley, M. J. Removing the stiffness from interfacial flow with surface tension. *J. Comp. Phys.* **114**, 312–338 (1994).
- Barabasi, A.-L. & Stanley, H. E. *Fractal Concepts in Surface Growth* (Cambridge Univ. Press, 1995).
- Haasen, P. *Physical Metallurgy* (Cambridge Univ. Press, 1986).
- Forty, A. J. in *Sir Charles Frank: An 80th Birthday Tribute* (ed. Chamber, R. G.) 164–187 (Adam Hilger, Bristol, 1991).
- Tulimieri, D. J., Yoon, J. & Chan, M. H. W. Ordering of helium mixtures in porous gold. *Phys. Rev. Lett.* **82**, 121–124 (1999).

Acknowledgements

This work was supported by the US Department of Energy, Basic Energy Sciences. The research of A.K. also benefited from computer time allocation at NU-ASCC. K.S. thanks the AFOSR for support.

Correspondence and requests for materials should be addressed to J.E (e-mail: Jonah.Erlebacher@jhu.edu).

Ice shelves in the Pleistocene Arctic Ocean inferred from glaciogenic deep-sea bedforms

Leonid Polyak*, Margo H. Edwards†, Bernard J. Coakley‡ & Martin Jakobsson§

* Byrd Polar Research Center, Ohio State University, Columbus, Ohio 43210, USA
 † Hawaii Mapping Research Group, Hawaii Institute of Geophysics and Planetology, University of Hawaii, Honolulu, Hawaii 96822, USA
 ‡ Department of Geology, Tulane University, New Orleans, Louisiana 70118, USA
 § Department of Geology and Geochemistry, Stockholm University, 106 91 Stockholm, Sweden

It has been proposed that during Pleistocene glaciations, an ice cap of 1 kilometre or greater thickness covered the Arctic Ocean^{1–3}. This notion contrasts with the prevailing view that the Arctic Ocean was covered only by perennial sea ice with scattered icebergs^{4–6}. Detailed mapping of the ocean floor is the best means to resolve this issue. Although sea-floor imagery has been used to reconstruct the glacial history of the Antarctic shelf^{7–9}, little data have been collected in the Arctic Ocean because of operational constraints^{10,11}. The use of a geophysical mapping system during the submarine SCICEX expedition in 1999¹² provided the opportunity to perform such an investigation over a large portion of the Arctic Ocean. Here we analyse backscatter images and sub-bottom profiler records obtained during this expedition from depths as great as 1 kilometre. These records show multiple bedforms indicative of glacial scouring and moulding of sea floor, combined with large-scale erosion of submarine ridge crests. These distinct glaciogenic features demonstrate that immense, Antarctic-type ice shelves up to 1 kilometre thick and hundreds of kilometres long existed in the Arctic Ocean during Pleistocene glaciations.

The central Arctic Ocean contains relatively shallow areas (water depths <1,000 m; see Fig. 1) on Yermak plateau, Lomonosov ridge and Chukchi borderland—which includes Chukchi plateau, Chukchi rise and Northwind ridge. During the SCICEX-99 expedition, conducted on the nuclear-powered submarine USS *Hawkbill*, shallow sea-floor areas were targeted for mapping to detect glaciogenic bedforms. Sea-floor images (collected using a submarine-mounted 12-kHz swath bathymetry and sidescan sonar¹²) from the Chukchi borderland and the Lomonosov ridge show a variety of bedforms, including random or subparallel scours, parallel lineations, and transverse ridges. On the records from the chirp sub-bottom profiler, these bedforms are associated with planed ridge crests with rough microrelief and obvious angular unconformities cut into the stratified sediments.

Randomly oriented furrows, typically <100-m wide and up to 30-m deep, densely cover the shallowest, <400-m-deep portions of sea floor on the Chukchi borderland and adjacent continental margin (Fig. 2a). Isolated larger scours up to 700-m wide and over 10-km long occur as deep as 500 m. Even greater depths, exceeding 900 m, are attained by closely spaced, subparallel scours on the Lomonosov ridge. Sea-floor scours are known to be formed by the drift of icebergs and pack-ice ridges¹³. At present, icebergs in the Arctic Ocean have at most 50-m draughts¹⁴, whereas icebergs off Antarctica and Greenland reach depths of 500–550 m (refs 15, 16). The largest depths of gouged sea floor, extending to 850 m, have been reported from the Yermak plateau¹⁰, matching the depth of scours on the Lomonosov ridge.

Below the depth range of dense scouring, the sea floor exhibits

† Present address: Center for Coastal Mapping, University of New Hampshire, Durham, New Hampshire 03824, USA.

coherent sets of evenly spaced, parallel, streamlined, low-relief lineations extending to 700-m depth on Chukchi borderland and to 1,000 m on Lomonosov ridge (Figs 2–4). At their shallow termination, these features are cross-cut and obscured by iceberg scours. The lineations have crest-to-crest spacing from <50 to 200 m and maximum lengths in excess of 15 km. These parallel, streamlined bedforms, or flutes, have not been observed previously in the central Arctic basin, but have been reported from surrounding glaciated shelves^{13,17–19} and around the Antarctic where they extend to 1,200-m depth^{7–9}. Flutes on Arctic shelves are relatively small, mostly under 30-m wide and 1-km long; whereas at the deep

Antarctic margin, the lineations are even larger than those discovered by SCICEX in the deep Arctic Ocean. The formation of such lineations has been explained by moulding of the soft bed by ice streams—the only known mechanisms for producing the sustained linear bedform fabric over large distances. Some fluted sites on Chukchi borderland include drumlin-like features that help to identify the direction of ice flow. Several large, almost 100-m-diameter blocks of sediment or rock with high acoustic return occur in the fluted area at the northern slope of Chukchi plateau (Fig. 2b); low-return ‘tails’ aligned with flutes indicate that these blocks were squeezed into sediment and dragged by ice.

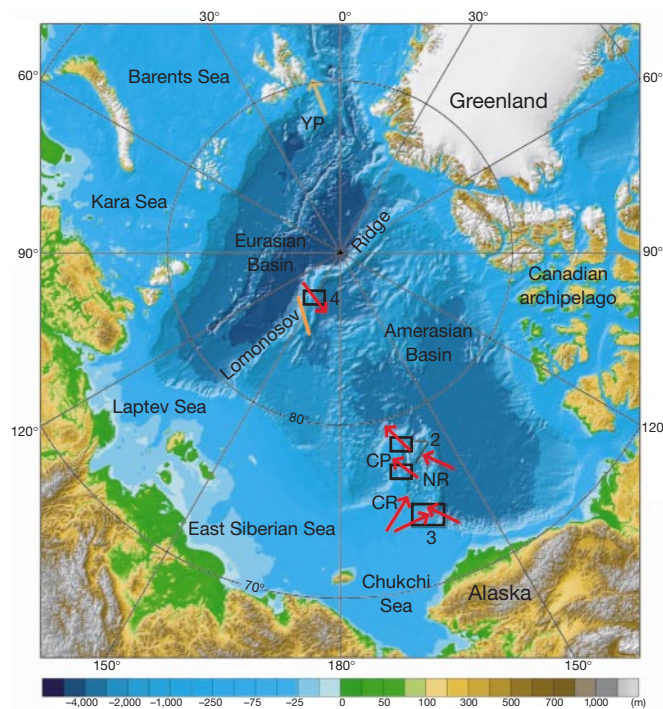


Figure 1 Map of the Arctic Ocean³⁰. Red arrows, reconstructed directions of ice-shelf flows; orange line, prevailing orientation of iceberg scours on Lomonosov ridge (this study, direction unresolved) and on Yermak plateau¹⁰. Numbered boxes show locations of

Figs 2–4. CP, Chukchi plateau; CR, Chukchi rise; NR, Northwind ridge; YP, Yermak plateau.

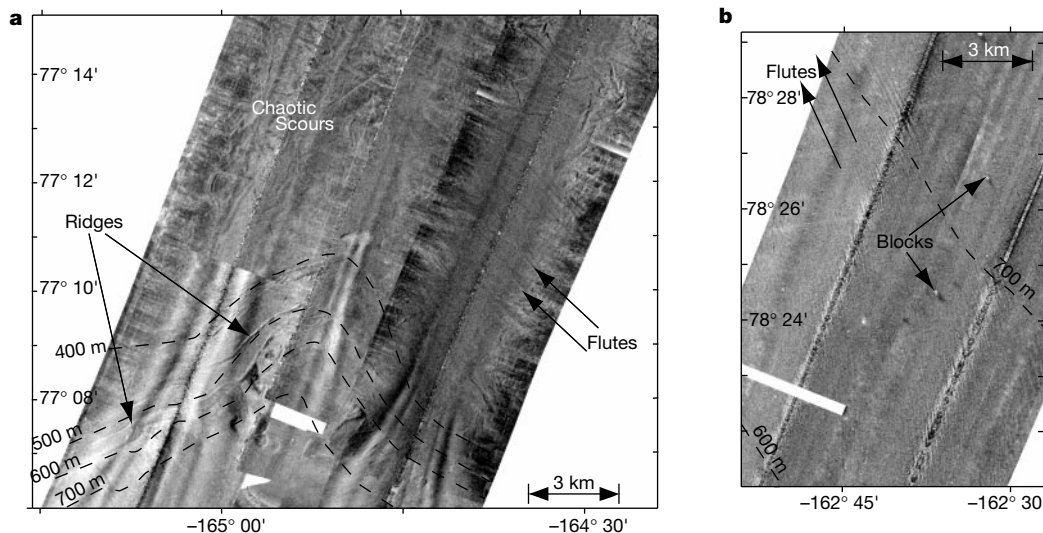


Figure 2 Swath sonar images from Chukchi plateau with overlain depth contour lines. Spatial resolution of gridded data is 16 m. **a**, Southern slope of the plateau with back-stepping ice-marginal ridges, northwest-trending flutes, and chaotic iceberg scours.

b, Northern slope of the plateau with northwest-trending flutes and scattered blocks of sediment/rock.

In several areas on Chukchi borderland, the fluted sea-floor pattern is complicated by nested sets of transverse, slightly sinuous or arcuate ridges reaching in excess of 100 m in width (Fig. 2a). These ridges parallel bathymetric contours, indicating that their formation was controlled by sea level. Such ridges are common for glaciated shelves, and have been interpreted to be formed by retreating ice-sheet margins (grounding lines)^{7,8,17–19}.

Identified bedforms from various sites can be tentatively correlated using their bathymetric position, orientation and preservation. Streamlined lineations are the best indicators of grounded ice flow^{7,8,17–19}. On Chukchi plateau, Northwind ridge, and the eastern slope of Chukchi rise, flutes consistently trend southeast–northwest (Fig. 1), with minor deviations on local topographic highs (Fig. 3). This orientation points at eastern Alaska and/or the western part of the Canadian Arctic archipelago as an ice-flow source. We suggest that the broad straits of the archipelago were the most likely outlets for major ice streams, consistent with glaciogenic features observed along the strait flanks^{20,21}. To the west, the Chukchi rise is covered by flutes that have a different orientation, indicative of ice movement from the Chukchi shelf (Figs 1, 3). These flutes do not extend to water depths >420 m, indicating thinner ice. From the overall regional pattern, we infer that a major ice shelf was propelled westwards by Alaskan/Canadian ice streams, but was deflected by the steep continental slope and/or by the Chukchi ice sheet and thus overran the Chukchi plateau in a northwest-trending direction. The general pattern of this ice movement over the Amerasian basin matches the distribution of ice-rafted debris deposited on the sea floor during glacial periods²².

The direction of ice flow across the fluted area on Lomonosov ridge is revealed in the chirp-sonar records (Figs 1, 4). Here, the crest is planed by erosion at a depth of almost 1,000 m; this planing occurs over a stretch at least 50-km wide, and a 20-m-thick lens of

acoustically transparent sediment descends from the eroded surface >100 m down the Amerasian flank of the ridge. The lens volume approximately matches the amount of sediment, with a maximum thickness of >50 m missing on top of the ridge as estimated by the projection of truncated strata. These features give a vivid picture of erosion of the crest by a single ice massif, moving north from the shelf of the Barents and Kara seas, with a debris lobe of reworked material pushed downslope on the lee side (Figs 1, 4). The dipping of the eroded surface towards the Eurasian side further shows that the ridge was a barrier to the passage of ice. The configuration of the eroded crest and the debris lobe, combined with the evenly fluted surface, indicate the sustained direction and strength of ice motion. The backstress of this motion had to be very high, at least equivalent to the ~600 kPa estimated for ice erosion on Yermak plateau³. These features suggest that the erosion on Lomonosov ridge was produced by a growing ice shelf rather than a random, abnormally large tabular iceberg, especially since the general Pleistocene iceberg drift in the Arctic Ocean was in the opposite direction²². Moreover, the fluted sea bed indicates an active grounded ice flow, not a ‘bulldozing’ action of icebergs. Similar large-scale erosional features occur on 500–550-m deep topographic highs on Northwind ridge, which have ~30-m thick, moraine-like, stacked lobes of acoustically transparent sediment on top. Orientation of these lobes attests to the motion of ice from the Alaskan/Canadian margin, consistent with the spatial distribution of flutes in the Chukchi region (Fig. 1).

The small ridges that are transverse to glacial lineations on Chukchi borderland probably mark the back-stepping of the ice-shelf grounding line with rising sea level during deglaciation (Fig. 2a)^{8,19}. These ridges do not occur at maximal water depths reached by flutes, which may indicate fast changes in ice-shelf profile during the initial stages of deglaciation. Iceberg scouring, which has obliterated the shallower bedforms reflecting the coherent ice

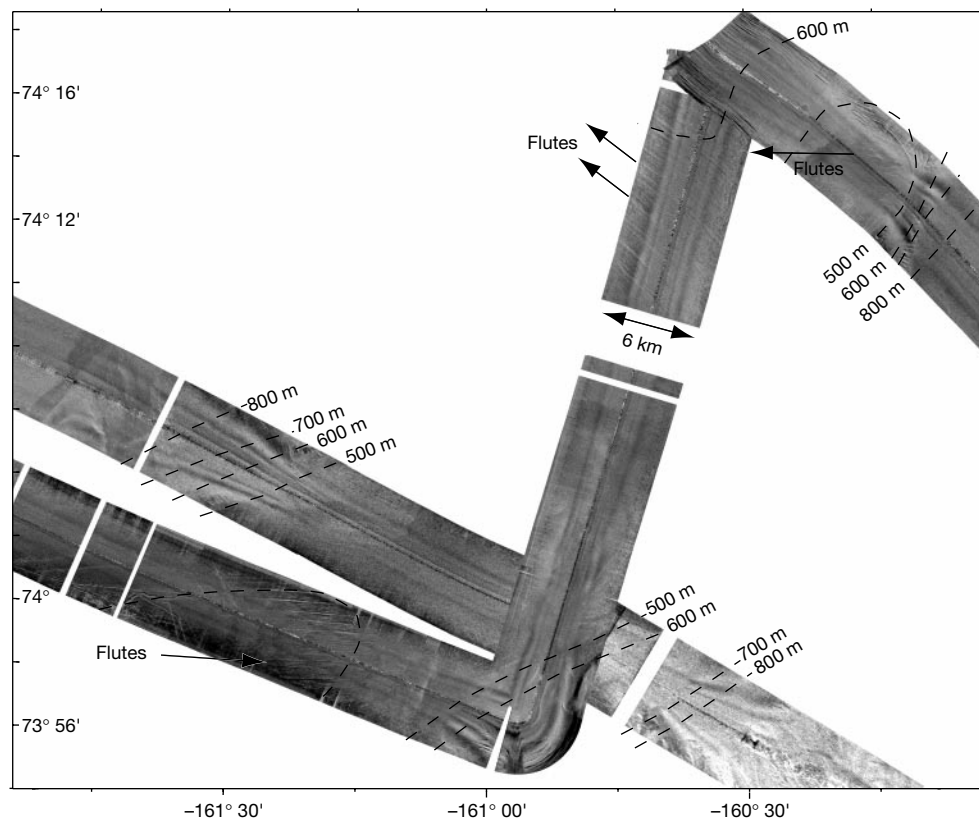


Figure 3 Swath sonar images from the eastern part of Chukchi rise with overlain depth contour lines. Spatial resolution of gridded data is 16 m. Two major sets of flutes point at the Chukchi shelf and at the Alaskan/Canadian margin as source areas. A local high

in the northeastern corner has a different orientation of flutes, presumably of younger age.

movement, represents conditions after the major ice-shelf disintegration. Subparallel scours at shallowest depths on Lomonosov ridge (750–950 m) indicate a flow of megabergs, possibly driven by a sustained current and/or jammed in an ice-bound Arctic Ocean, as suggested for similar features on Yermak plateau^{10,23}. Random scouring at yet shallower depths of <350–400 m in the Chukchi area reflects unrestricted movement of minor icebergs driven by winds and/or currents.

The stratigraphic boundary formed by glacial erosion on Lomonosov ridge (Fig. 4) has been recovered by coring²⁴. This erosion was interpreted to occur at the end of marine isotopic stage (MIS) 6, approximately 150 kyr ago. According to another, more conventional, age model for the Arctic Ocean sediments⁶, this stratigraphic level has a much older age of >600 kyr (MIS 16). The latter interpretation is consistent with an estimate of ~660 kyr ago for the timing of glacial grounding on Yermak plateau²⁵ and with the period of maximal glacial erosion of the Barents Sea between about 1,000 and 440 kyr ago²⁶.

In the absence of stratigraphic control for glaciogenic features on Chukchi borderland, we cannot conclude whether or not they were coeval with ice grounding on Lomonosov ridge. Moreover, the multitude of glaciogenic bedforms may represent a composite of several glacial events with a similar pattern of ice flow over Chukchi

borderland. Deviation of flutes on local shallows from the general orientation (Fig. 3) indicates the likelihood of multiple ice advances. However, we may be able to find direct evidence for only the thickest ice shelves; this is because thin ice would not reach the deep sea floor, and ice-flow markings in the shallowest areas would be obliterated by chaotic iceberg scouring.

An unfossiliferous, overcompacted sediment deposited before 13 kyr ago at ~400-m depth on Chukchi rise²⁷ possibly indicates ice grounding during the Last Glacial Maximum. The existence of an extensive ice shelf is corroborated by extremely low sedimentation rates (possibly a hiatus) and the absence of biogenic remains in sediments throughout the Amerasian basin during 13–20 kyr ago^{27,28}. We presume that the removal of this ice shelf facilitated large-scale surges upstream, such as a catastrophic discharge of 80,000 km³ of ice from the northwestern part of the Canadian archipelago before 10 kyr ago²¹. Understanding this and older events associated with growth and disintegration of Arctic ice shelves will help explain the behaviour of the West Antarctic Ice Sheet²⁹ and, in broader perspective, the stability of glacial climates. Ice shelves in the Arctic have large potential effects on climate by affecting the albedo and ocean–atmosphere heat exchange; this highlights a significant unresolved question—was the entire Arctic Ocean covered by a continuous ice shelf at some time during the Pleistocene? To answer this question further mapping of glaciogenic bedforms and their stratigraphic investigation are required; this could establish whether ice-shelf advances were synchronous in various parts of the Arctic basin. □

Received 21 August; accepted 22 December 2000.

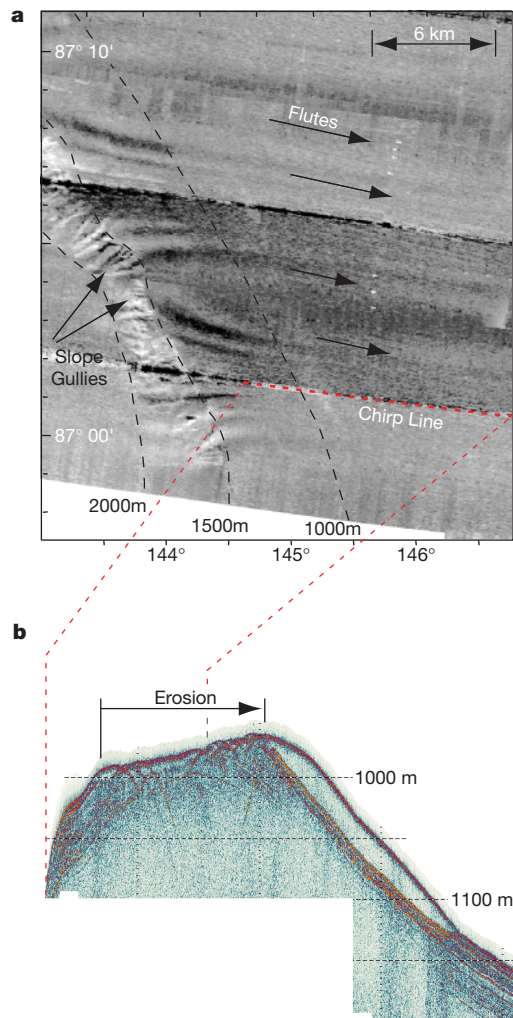


Figure 4 Swath sonar and chirp images from Lomonosov ridge. Spatial resolution of gridded sidescan data (a) is 21 m; vertical resolution of the chirp data (b) is tens of centimetres. The planed, eroded top surface of the crest is covered with ESE-trending low-relief flutes. The acoustically transparent debris lens drapes the lee (Amerasian) slope of the ridge.

- Mercer, J. H. A former ice sheet in the Arctic Ocean? *Palaeogeogr. Palaeoclimatol. Palaeoecol.* **8**, 19–27 (1970).
- Lindstrom, D. R. & MacAyeal, D. R. Scandinavian, Siberian, and Arctic Ocean glaciation: effect of Holocene atmospheric CO₂ variations. *Science* **245**, 628–631 (1989).
- Grosswal, M. G. & Hughes, T. J. The case for an ice shelf in the Pleistocene Arctic Ocean. *Polar Geogr.* **23**, 23–54 (1999).
- Clark, D. L. Origin, nature, and world climate effect of Arctic Ocean ice cover. *Nature* **300**, 321–325 (1980).
- Phillips, R. L. & Grantz, A. Quaternary history of sea ice and paleoclimate in the Amerasia basin, Arctic Ocean, as recorded in the cyclical strata of Northwind Ridge. *Geol. Soc. Am. Bull.* **109**, 1101–1115 (1997).
- Spielhagen, R. F. *et al.* Arctic Ocean evidence for late Quaternary initiation of northern Eurasian ice sheets. *Geology* **25**, 783–786 (1997).
- Anderson, J. B. *Antarctic Marine Geology* (Cambridge Univ. Press, Cambridge, 1999).
- Shipp, S., Anderson, J. & Domack, E. Late Pleistocene–Holocene retreat of the West Antarctic Ice-Sheet system in the Ross Sea: Part 1—Geophysical results. *Geol. Soc. Am. Bull.* **111**, 1486–1516 (1999).
- Canals, M., Urgeles, R. & Calafat, A. M. Deep sea-floor evidence of past ice streams off the Antarctic Peninsula. *Geology* **28**, 31–34 (2000).
- Vogt, P. R., Crane, K. & Sundvor, E. Deep Pleistocene iceberg plowmarks on the Yermak Plateau: sidescan and 3.5 kHz evidence for thick calving ice fronts and a possible marine ice sheet in the Arctic Ocean. *Geology* **22**, 403–406 (1994).
- Jakobsson, M. First high-resolution chirp sonar profiles for the central Arctic Ocean reveal erosion of Lomonosov Ridge sediments. *Mar. Geol.* **158**, 111–123 (1999).
- Edwards, M. H. *et al.* Evidence of recent volcanic activity on the ultra-slow spreading Gakkel Ridge. *Nature* **409**, 808–812 (2001).
- Davies, T. A. *et al.* (eds) *Glaciated Continental Margins: an Atlas of Acoustic Images* (Chapman and Hall, London, 1997).
- Robe, R. Q. in *Dynamics of Snow and Ice Masses* (ed. Colbeck, S. C.) 211–259 (Academic, New York, 1980).
- Barnes, P. W. & Lien, R. Iceberg rework shelf sediments to 500 m off Antarctica. *Geology* **16**, 1130–1133 (1988).
- Dowdeswell, J. A., Villinger, H., Whittington, R. J. & Marienfeld, P. Iceberg scouring in Scoresby Sund and on the East Greenland continental shelf. *Mar. Geol.* **111**, 37–53 (1992).
- Josenhans, H. W. & Zevenhuizen, J. Dynamics of the Laurentide Ice Sheet in the Hudson Bay, Canada. *Mar. Geol.* **92**, 1–26 (1990).
- Solheim, A., Russwurm, L., Elverhøi, A. & Nyland-Berg, M. Glacial geomorphic features in the northern Barents Sea: direct evidence for grounded ice and implications for the pattern of deglaciation and late glacial sedimentation. *Geol. Soc. Spec. Publ.* **53**, 253–268 (1990).
- Polyak, L., Forman, S. L., Herlihy, F. A., Ivanov, G. & Krinitsky, P. Late Weichselian deglacial history of the Svyataya (Saint) Anna Trough, northern Kara Sea, Arctic Russia. *Mar. Geol.* **143**, 169–188 (1997).
- Dyke, A. S., Morris, T. F., Green, D. E. C. & England, J. Quaternary geology of Prince of Wales Island, Arctic Canada. *Geol. Surv. Can. Mem.* **433** (1992).
- Clark, C. D. & Stokes, C. R. Extent and basal characteristics of the M’Clintock Channel ice stream. *Quat. Int.* (in the press).
- Bischof, J. F. & Darby, D. A. Mid- to Late Pleistocene ice drift in the Western Arctic Ocean: evidence for a different circulation in the past. *Science* **277**, 74–78 (1997).
- Vogt, P. R., Crane, K. & Sundvor, E. Deep Pleistocene iceberg plowmarks on the Yermak Plateau: sidescan and 3.5 kHz evidence for thick calving ice fronts and a possible marine ice sheet in the Arctic Ocean (reply). *Geology* **23**, 477–478 (1995).

24. Jakobsson, M. *et al.* Pleistocene stratigraphy and paleoenvironmental variation from Lomonosov Ridge sediments, central Arctic Ocean. *Global Planet. Change* (in the press).
 25. Flower, B. P. Overconsolidated section on the Yermak Plateau, Arctic Ocean: ice sheet grounding prior to ca. 660 ka? *Geology* **25**, 147–150 (1997).
 26. Faleide, J. J. *et al.* Late Cenozoic evolution of the western Barents Sea-Svalbard continental margin. *Glob. Planet. Change* **12**, 53–74 (1996).
 27. Darby, D. A., Bischof, J. F. & Jones, G. A. Radiocarbon chronology of depositional regimes in the western Arctic Ocean. *Deep-Sea Res. II* **44**, 1745–1757 (1997).
 28. Poore, R. Z., Osterman, L., Curry, W. B. & Phillips, R. L. Late Pleistocene and Holocene meltwater events in the western Arctic Ocean. *Geology* **27**, 759–762 (1999).
 29. Oppenheimer, O. Global warming and the stability of the West Antarctic Ice Sheet. *Nature* **393**, 325–332 (1998).
 30. Jakobsson, M., Cherkis, N., Woodward, J., Coakley, B. J. & Macnab, R. A new grid of Arctic bathymetry: a significant resource for scientists and mapmakers. *Eos* **81**, 89, 93, 96 (2000).

Acknowledgements

We thank R. Perry (the captain), the officers and crew of the USS *Hawkbill* and the scientists and engineers who sailed during SCICEX-99; we also thank P. Johnson for assistance with figures. This work was supported by the US NSF.

Correspondence and requests for materials should be addressed to L.P. (e-mail: polyak.1@osu.edu).

Geochemical tracing of Pacific-to-Atlantic upper-mantle flow through the Drake passage

J. A. Pearce*, P. T. Leat†, P. F. Barker† & I. L. Millar†

* Department of Earth Sciences, Cardiff University, Cardiff, CF10 3YE, UK

† British Antarctic Survey, Cambridge CB3 0ET, UK

The Earth's convecting upper mantle can be viewed as comprising three main reservoirs, beneath the Pacific, Atlantic and Indian oceans. Because of the uneven global distribution and migration of ridges and subduction zones, the surface area of the Pacific reservoir is at present contracting at about 0.6 km² yr⁻¹, while the Atlantic and Indian reservoirs are growing at about 0.45 km² yr⁻¹ and 0.15 km² yr⁻¹, respectively^{1,2}. Garfunkel¹ and others have argued that there must accordingly be net mantle flow from the Pacific to the Atlantic and Indian reservoirs (in order to maintain mass balance), and Alvarez² further predicted that this flow should be restricted to the few parts of the Pacific rim (here termed 'gateways') where there are no continental roots or subduction zones that might act as barriers to shallow mantle flow. The main Pacific gateways are, according to Alvarez^{2,3}, the south-east Indian Ocean, the Caribbean Sea and the Drake passage. Here we report geochemical data which confirm that there has been some outflow of Pacific mantle into the Drake passage—but probably in response to regional tectonic constraints, rather than global mass-balance requirements. We also show that a mantle domain boundary, equivalent to the Australian–Antarctic discordance, must lie between the Drake passage and the east Scotia Sea.

Figure 1b and c shows the distribution of the ~10⁶ km² of new oceanic crust created between South America and Antarctica since sea-floor spreading began in the Drake passage (gateway d in Fig. 1a) about 30 Myr ago^{4,5}. Most oceanic crustal accretion took place in the Drake passage itself (about 30–10 Myr ago), the central Scotia Sea (about 20–10 Myr ago), and the east Scotia Sea (≤ 10 Myr ago). The adjacent Antarctic–Phoenix ridge was also active over much of this period (> 30 Myr ago to about 4 Myr ago). This whole 30-Myr period is thought to have been marked by westward subduction of Atlantic oceanic crust and eastward roll-back of the subducting slab.

A central question has been whether or not this roll-back is a consequence of eastward Pacific mantle flow.

Figure 1c gives the locations of samples that we have analysed. Dredges DR.62 and 63 recovered old crust from the Drake passage, and DR.7 recovered the youngest crust. DR.12 recovered old crust from the east Scotia Sea, and DR.20, 23, 107 and 118 the youngest crust. DR.3 recovered the youngest crust from the Antarctic–Phoenix ridge⁶. Our geochemical data are listed in Table 1. To assess which crust was generated from Pacific mantle, and which from Atlantic mantle, we adopt the method of isotope fingerprinting of basalts that has been used successfully to study the southeast Indian gateway (that is, the Australian–Antarctic discordance or AAD; see, for example, refs 7–9).

Figure 2a and b show two of the most effective projections for discriminating between mantle domains: plots of ²⁰⁸Pb/²⁰⁴Pb ratios versus ²⁰⁶Pb/²⁰⁴Pb ratios, and ¹⁴³Nd/¹⁴⁴Nd versus ²⁰⁶Pb/²⁰⁴Pb. The Pacific domain, which extends beneath much of the Pacific Ocean, is defined here just by data from the southeast Pacific—namely, the East Pacific Rise south of the Equator^{10,11}, the Pacific–Antarctic ridge^{12–14}, and the Chile ridge^{15,16}, excluding anomalous values at the ridge–trench intersection. We have divided the South Atlantic mantle into three domains, according to geochemical coherence and proximity to hotspots. The Bouvet domain extends from Bouvet Island along the southwest Indian ridge to the west, along the South-America–Antarctic ridge to the east, and for a short distance up the Mid-Atlantic Ridge^{17–19}. The Shona and Discovery domains encompass the Mid-Atlantic Ridge²⁰ further north (Fig. 1b). It is apparent that the Pacific domain is distinct from the three Atlantic domains in its high ¹⁴³Nd/¹⁴⁴Nd and low ²⁰⁸Pb/²⁰⁴Pb for a given ²⁰⁶Pb/²⁰⁴Pb, combined with its negative trend on the Nd–Pb plot and positive trend on the Pb–Pb plot. The Bouvet and Shona domains give trends similar to, but displaced from, the Pacific domain. The Discovery domain extends slightly into the Pacific domain, but forms a trend orthogonal to it.

Of our new data, the samples from the east Scotia Sea plot in the Atlantic (Bouvet) field on both diagrams (Fig. 2c, d). They have lower ²⁰⁶Pb/²⁰⁴Pb ratios than the samples from the South-America–Antarctic ridge, which reflects their greater distance from the Bouvet plume. By contrast, sample DR.7 from the Drake passage ridge plots

Table 1 Analyses from the Drake passage and surrounding region

Sample (DR.)	Location	⁸⁷ Sr/ ⁸⁶ Sr	¹⁴³ Nd/ ¹⁴⁴ Nd	²⁰⁸ Pb/ ²⁰⁴ Pb	²⁰⁷ Pb/ ²⁰⁴ Pb	²⁰⁶ Pb/ ²⁰⁴ Pb
62.B	DPM	0.70421	0.51286	18.992	15.621	39.028
62.153	DPM	0.70469	0.51317	18.303	15.512	37.875
63.2	DPM	0.70312	0.51294	18.850	15.584	38.465
63.20	DPM	0.70312	0.51295	18.632	15.594	38.456
3.2	APR	0.70283	0.51307	18.592	15.544	38.040
3.7	APR	0.70263	0.51310	18.371	15.526	37.888
3.4	APR	0.70350	0.51305	18.611	15.535	38.187
7.3	DPR	0.70274	0.51316	18.227	15.514	37.723
12.19	ESM	0.70309	0.51303	18.716	15.602	38.535
WX.2	ESR2	0.70289	0.51306	18.223	15.528	37.938
20.36	ESR3	0.70285	0.51308	18.115	15.493	37.733
23.1	ESR9	0.70297	0.51304	18.024	15.496	37.726
107.1	ESR1	0.70305	0.51310	17.905	15.482	37.580
118.3	ESR1	0.70325	0.51304	18.211	15.551	37.874

Isotope analyses of basic volcanic rocks from the Drake passage margin (DPM), Antarctic–Phoenix ridge (APR), Drake passage ridge (DPR), east Scotia Sea margin (ESM) and east Scotia ridge (ESR_n where n is the segment number²¹). Ages are 28 Myr for the DPM samples, 10 Myr for the DPR and ESM samples, and <1 Myr for the ESR samples. Samples from the APR, DPR and DR.62.153 are MORBs, other samples from the DPM are tholeiitic (DR.63.20) and alkalic (DR.62.B and DR.63.2) ocean island basalts, samples from the ESR are MORBs with negligible to small subduction components, and the sample from the ESM is a MORB with a more significant subduction component. All analyses are new and on dredge (DR.) samples except for that from the wax-core glass (WX.20) which is published²² and included for comparison. Isotope ratios are by thermal ionization mass spectrometer²³. Over the period of this work, three analyses of NBS987 gave Sr isotope ratios of 0.710198 ± 0.000022 (2σ) and the data were normalized to 0.710240. Five analyses of the La Jolla standard gave Nd isotope ratios of 0.511900 ± 0.000022 (2σ) and the data were normalized to 0.511864. Pb isotope ratios were corrected for fractionation using the replicate analyses of the NBS981 standard. Sr and Nd isotope ratios have internal precisions (1 s.e.) of ± (3–4) × 10⁻⁶ and ± (6–8) × 10⁻⁶ respectively, and Pb isotope ratios have internal precisions of ± (1–2) × 10⁻⁶ (6/4 and 7/4) and ± (2–4) × 10⁻³ (8/4). See Table 1 in Supplementary Information for dredge depths and locations, and for the X-ray fluorescence major-element and inductively-coupled plasma mass spectrometer trace-element analyses.